Poloidal ULF wave observed in the plasmasphere boundary layer

W. Liu,[1,2] J. B. Cao,[1,2] X. Li,[3] T. E. Sarris,[4] Q.-G. Zong,[5] M. Hartinger,[6] K. Takahashi,[7] H. Zhang,[8] Q. Q. Shi,[9] and V. Angelopoulos[10]

Received 18 April 2013; revised 22 June 2013; accepted 28 June 2013; published 23 July 2013.

[1] We report on a rare ultra-low-frequency (ULF) wave generation event associated with the formation of a plasmasphere boundary layer (PBL), which was well observed by one of the THEMIS satellites, TH-D, during subsequent outbound passes. On 13 September 2011, TH-D observed a sharp plasmapause at L = 3.4. The plasmasphere started to expand and continued to be refilled on 14 September. On 15 September, a PBL was formed with two density gradients at L = 4.4 and 6.5, respectively. Within the two density gradients, strong radial magnetic field and azimuthal electric field oscillations were observed, suggesting poloidal ULF waves. Based on the phase delay between magnetic and electric field signals, as well as the comparison between the observed wave frequency and predicted harmonic eigenfrequency, we find that the observed oscillations are second harmonic poloidal waves. Further investigation shows that the observed waves are likely generated by drift-bounce resonance with "bump-on-tail" plasma distributions at ~10 keV. We demonstrate that the waves are excited within the PBL where the eigenfrequency is close to the bounce frequency of these hot protons, but not outside the PBL where the eigenfrequency deviates from the bounce frequency. Finally, we suggest that cold plasma density seems to be a controlling factor for ULF wave generation as well, in addition to the bump-on-tail energy source, by altering eigenfrequency of the local field lines.

Citation: Liu, W., J. B. Cao, X. Li, T. E. Sarris, Q.-G. Zong, M. Hartinger, K. Takahashi, H. Zhang, Q. Q. Shi, and V. Angelopoulos (2013), Poloidal ULF wave observed in the plasmasphere boundary layer, *J. Geophys. Res. Space Physics*, *118*, 4298–4307, doi:10.1002/jgra.50427.

1. Introduction

[2] The plasmasphere contains cold plasma extended from the Earth's ionosphere. The plasmapause is identified as a boundary where the density of cold plasma decreases sharply. Based on CRRES observations, however, *Moldwin et al.* [2002] found that "classic" isolated steep density gradients can be seen in only 16% of the plasmapause crossings. In most cases, instead, significant density structure was observed outside the innermost steep density gradient. The concept "plasmasphere boundary layer" (PBL) was thus suggested by *Carpenter and Lemaire* [2004] to refer to a plasmapause region with complexity and variable plasma populations.

[3] In a statistical view, a good correlation has been reported between the inner edge of the outer electron radiation belt and the minimum plasmapause location [*Li et al.*, 2006]. This has been explained by the fact that it is difficult to energize electrons inside the plasmapause, where losses still occur due to pitch angle scattering by electromagnetic ion cyclotron waves and plasmaspheric hiss waves. However, the effects of the PBL on the acceleration and loss of radiation belt electrons have not been well understood, mainly because of the lack of information about wave characteristics within the PBL [*Moldwin and Zou*, 2012].

[4] The ultra-low-frequency (ULF) waves are the oscillations in the Earth's magnetic field in the frequency range of 1 mHz to 1 Hz. The terms "poloidal" and "toroidal" modes are used for standing Alfvén waves with magnetic field (and plasma bulk motion) oscillations in the radial and azimuthal directions (or the corresponding azimuthal and radial electric field), respectively. For the poloidal mode in the Pc4 (6.7–22 mHz) and Pc5 (1.7–6.7 mHz) bands studied in this paper, several generation mechanisms have been suggested after decades of study, including drift resonance

[1]Space Science Institute, School of Astronautics, Beihang University, Beijing, China.
[2]State Key Laboratory of Space Weather, Chinese Academy of Sciences, Beijing, China.
[3]Laboratory for Atmospheric and Space Physics, University of Colorado Boulder, Boulder, Colorado, USA.
[4]Space Research Laboratory, Democritus University of Thrace, Xanthi, Greece.
[5]Institute of Space Physics and Applied Technology, Peking University, Beijing, China.
[6]Atmospheric, Oceanic, and Space Sciences Department, University of Michigan, Ann Arbor, Michigan, USA.
[7]The Johns Hopkins University Applied Physics Laboratory, Laurel, Maryland, USA.
[8]Institute of Geology and Geophysics, Chinese Academy of Sciences, Beijing, China.
[9]School of Space Science and Physics, Shandong University at Weihai, Weihai, China.
[10]Institute of Geophysics and Planetary Physics, University of California, Los Angeles, California, USA.

Corresponding author: W. Liu, Space Science Institute, School of Astronautics, Beihang University, Xueyuan Road, 37, Beijing 100191, China (liuwenlong@buaa.edu.cn)

2169-9380/13/10.1002/jgra.50427

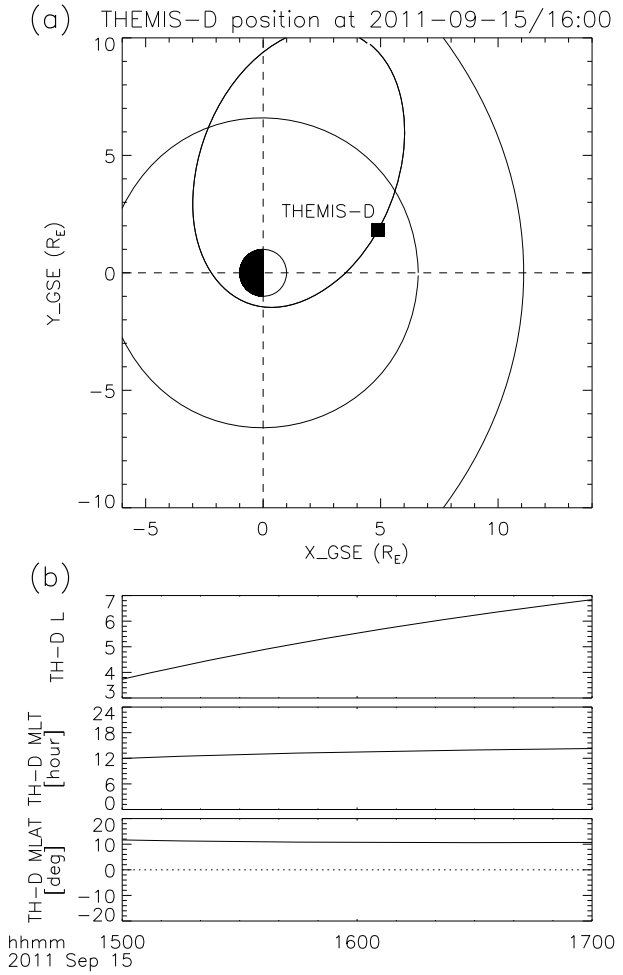

Figure 1. (a) Orbit of TH-D in the GSE X-Y plane on 15 September 2011, magnetopause is plotted based on the *Shue et al*. [1998] model with solar wind $D_p = 1.2$ nPa and IMF $B_z = 0$ nT; (b) The L value, magnetic local time, and magnetic latitude of TH-D from 15:00 to 17:00 UT on 15 September 2011.

[*Southwood*, 1976], drift-bounce resonance [*Southwood*, 1976; *Hughes et al*., 1978], impact of interplanetary shocks [*Zong et al*., 2009a; *Sarris et al*., 2010], Alfvén oscillations with high azimuthal numbers [*Kozlov et al*., 2006; *Leonovich et al*., 2008], and activity in the magnetotail [*Cao et al*., 2008, 2010].

[5] ULF oscillations can be excited at different harmonics. The second harmonic poloidal oscillation is a frequently observed phenomenon in the inner magnetosphere and has been extensively studied theoretically [e.g., *Southwood*, 1976; *Chen and Hasegawa* 1991] and by analyzing spacecraft measurements [e.g., *Hughes et al*., 1978; *Arthur and McPherron*, 1981; *Singer et al*., 1982; *Anderson et al*., 1990; *Takahashi et al*., 1990, *Takahashi and Anderson*, 1992; *Baddeley et al*., 2004, 2005a]. It has been well accepted that second harmonic poloidal waves are generated mainly by the drift-bounce resonance with free energy from a bump-on-tail ion distribution.

[6] In order to identify the harmonic mode of a poloidal oscillation, two methods are usually used based on spacecraft measurements [*Singer et al*., 1982]. The first method compares the phase difference between radial magnetic field B_r (positively outwards) and azimuthal electric field E_ϕ (positively eastwards) [*Singer et al*., 1982; *Takahashi et al*., 2011]. The phase of E_ϕ leads (lags) B_r by 90° for even (odd) harmonic mode for the measurements made slightly north of the magnetic equator. Thus, simultaneous measurements of magnetic and electric field can be used to identify the harmonic of a poloidal wave. The second method compares the observed wave frequency with the field line eigenfrequency calculated theoretically. The decoupled transverse wave equations can be solved numerically with a specified magnetic field model and boundary conditions. For example, *Cummings et al*. [1969] calculated the eigenfrequencies of standing Alfvén waves for different harmonics at geosynchronous orbit with assumptions of dipole magnetic field and perfectly conducting ionospheres. *Orr and Matthew* [1971] used similar assumptions but expanded the calculation to other L values. More solutions with different assumptions were subsequently published, such as the solutions with considerations of finite ionospheric conductivity [*Newton et al*., 1978] and realistic magnetic field model [*Singer et al*., 1981].

[7] In this paper, we present a rare poloidal ULF wave event that is observed within the PBL region by the THEMIS spacecraft [*Angelopoulos*, 2008]. The evolution of the PBL is investigated based on observations of three consecutive outbound passes. We find that the observed poloidal oscillations are second harmonic waves generated by drift-bounce resonance. We demonstrate that cold plasma density plays an important role in regulating ULF wave generation by altering field line eigenfrequencies. The remainder of this paper is organized as follows. In section 2, we introduce the orbit of the satellite and the data set used in this study. In section 3, we present the satellite observations. In section 4, we discuss on the observations, followed by our conclusions in section 5.

2. Orbit and Data Set

[8] The THEMIS mission includes five identical satellites (TH-A through TH-E), launched into near equatorial orbits on 17 February 2007, providing multipoint observations through the inner magnetosphere. Observations used in this study are obtained by one of the inner probes, TH-D, from 13 to 15 September 2011. Figure 1a plots the orbit of TH-D on 15 September 2011 with an apogee of 12 R_E and a perigee of 1.5 R_E. The probe was outbound in the dayside near the noon sector during this event.

[9] More detailed orbital information is plotted in Figure 1b, including the time series of L value [*McIlwain*, 1961], magnetic local time (MLT) and magnetic latitude (MLAT) from top to bottom, respectively. It is shown that, from 15:00 to 17:00 UT, TH-D crossed a region of 3.7 to 6.8 in L shell and 12 to 14 in MLT. The MLAT of TH-D was around 11° during this time period, which suggests that TH-D was situated north of the magnetic equator. This information is critical in interpreting the harmonic mode for in situ measurements of ULF waves, which will be further discussed later.

[10] The measurements used in this study are from the Fluxgate Magnetometer (FGM) [*Auster et al*., 2009], the Electric Field Instrument (EFI) [*Bonnell et al*., 2008], and

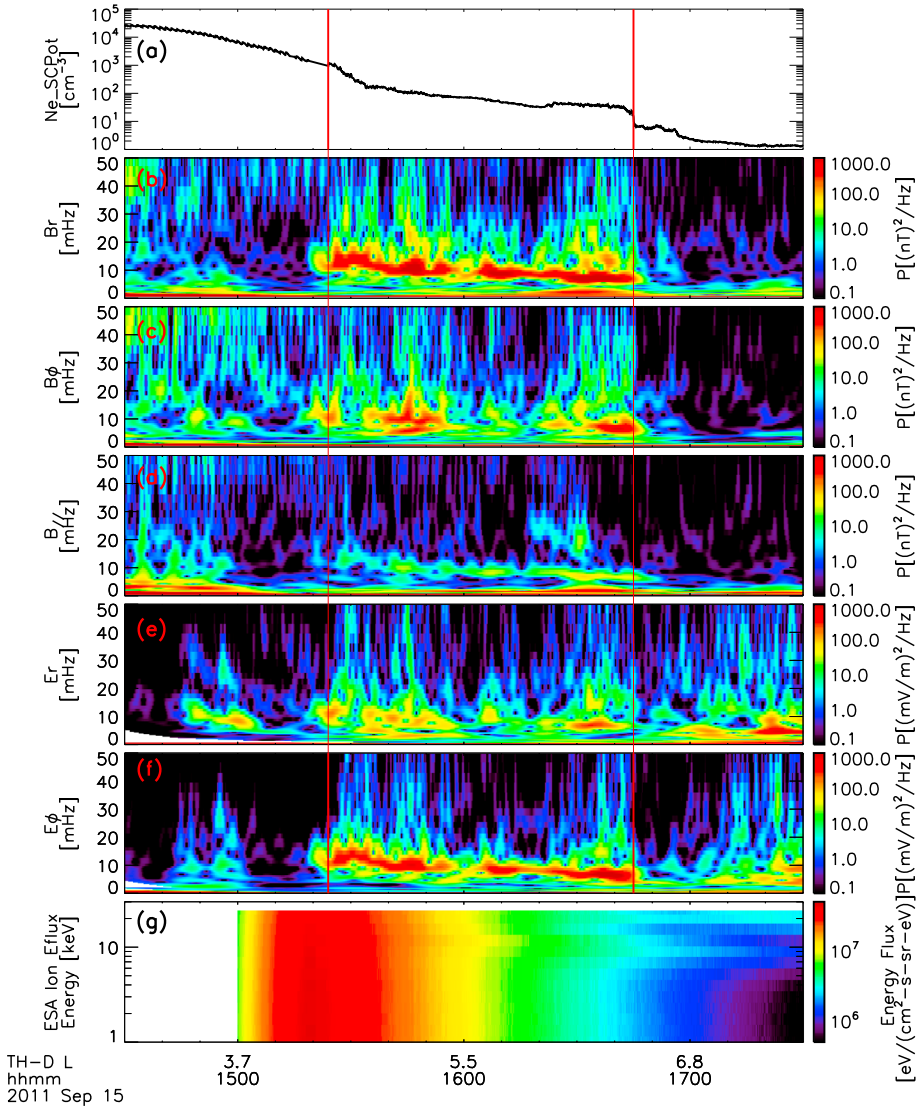

Figure 2. Observations by TH-D on 15 September 2011: (a) Electron density derived from the spacecraft potential measurement; (b–f) wavelet power spectra of magnetic field (b: radial, c: azimuthal, d: parallel), and electric field (e: radial, f: azimuthal) components in the MFA coordinate system; (g) spectra of ion energy flux between 1 and 30 keV.

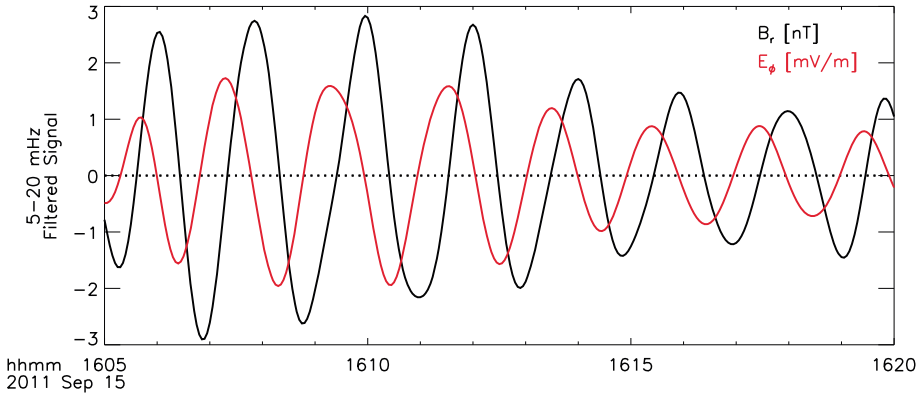

Figure 3. Band-pass-filtered signals of radial magnetic field (black line) and azimuthal electric field (red line) within 5–20 mHz observed by TH-D.

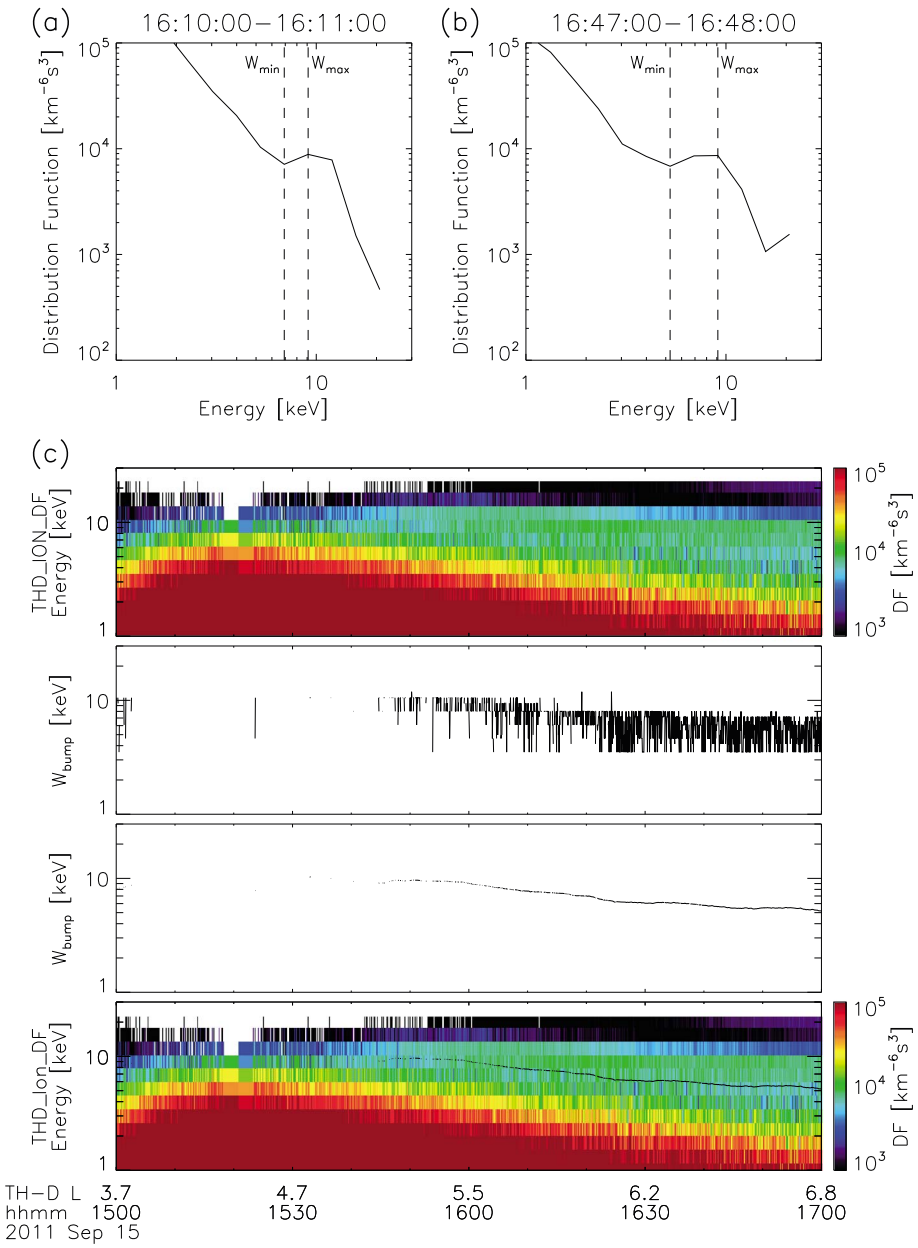

Figure 4. (a) Ion distribution functions measured at 16:00 UT by TH-D on 15 September 2011; (b) Same as Figure 4a but for 16:47 UT; (c) Measured ion distribution functions, energy at the bump-on-tail distribution W_{bump}, smoothed W_{bump} with a 10 min running window, and the comparison between W_{bump} and ion distribution function spectra are plotted from top to bottom panels, respectively.

the Electrostatic Analyzers (ESA) [*McFadden et al*., 2008] onboard the THEMIS probes. Magnetic field and electric field data used here have a time resolution of about 3 s, corresponding to the spin period of the spacecraft. This time resolution is sufficient for capturing features of waves with frequencies up to 167 mHz (the Nyquist frequency). EFI provides electric field measurements in the two components in the spin plane of the spacecraft (close to the GSE x-y plane [*Angelopoulos*, 2008]). The third (axial) component of electric field can be estimated under the assumption that $\mathbf{E} \cdot \mathbf{B} = 0$ [*Bonnell et al*., 2008]. This technique allows one to transform the electric field from the spacecraft coordinate system into other coordinate systems. If the magnetic field is close to parallel to the spin plane, the error associated with this method grows, leading to a ten-to-one increase in error for angles between the spin plane and the background magnetic field smaller than ~6°, as estimated by *Bonnell et al*. [2008]. In our study, the error introduced by this method is negligible because the angle between the spin plane and the background magnetic field is 50–60° for TH-D during this event.

[11] Magnetic and electric field measurements are transformed into the Mean Field Aligned (MFA) coordinate system with three components in the radial (r), azimuthal (ϕ) and parallel (//) directions [e.g., *Liu et al*., 2009]. In this study, $B_{//}$ is obtained from a 30 min running average of the magnetic field, centered at the data point being processed. The azimuthal direction $\mathbf{e}_{\varphi}$ is determined by $\hat{\mathbf{e}}_{//} \times \vec{\mathbf{r}}_e$,

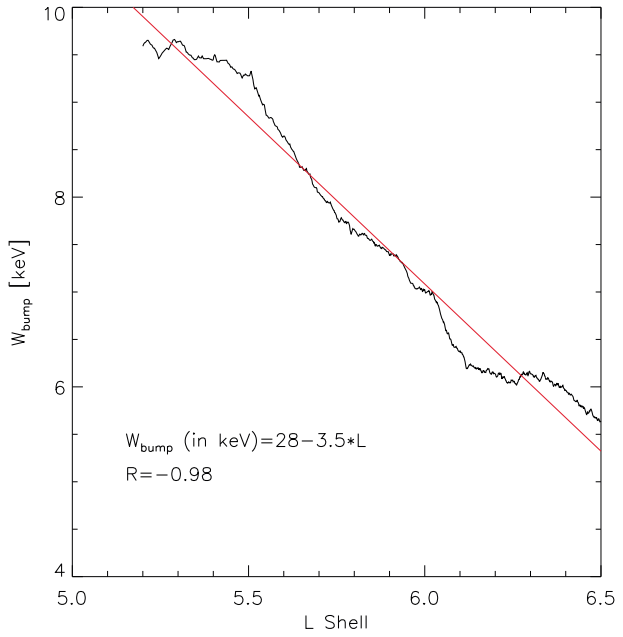

Figure 5. Observed W_{bump} as a function of L value is plotted in black and the result of a linear fit is plotted in red.

positively eastwards, where $\hat{\mathbf{e}}_{//}$ points along the average background magnetic field direction and $\vec{\mathbf{r}}_e$ is the radial position vector, positively outwards. The radial direction $\hat{\mathbf{e}}_r$, positively outwards, is defined to let the vectors ($\hat{\mathbf{e}}_r$, $\hat{\mathbf{e}}_\varphi$, $\hat{\mathbf{e}}_{//}$) complete an orthogonal system.

3. Observations

3.1. Observations of a Poloidal Wave Event on 15 September 2011

[12] Overview parameters during this event are plotted in Figure 2. In the first panel, the electron density derived from spacecraft potential measurements is plotted. Spacecraft potential is the result of the balance between photo-ionization on the spacecraft and neutralization by ambient plasma. One can generally derive electron density from spacecraft potential with an uncertainty of a factor of 2 [*Pedersen et al*., 1998]. This precision is sufficient for identifying plasmapause structures and has been used in several studies [e.g., *Li et al*., 2010]. From Figure 2a, we can see that there are two density drops at L = 4.4 and L = 6.5, respectively, suggesting the presence of a PBL.

[13] The wavelet power spectra of B_r, B_ϕ, $B_{//}$, E_r, and E_ϕ from TH-D are plotted in panels b through f, respectively. Strong narrowband wave power is clearly seen in both the B_r and E_ϕ components, suggesting the existence of a poloidal ULF wave. The frequency of this wave gradually decreases from 15 to 5 mHz as the spacecraft moves outward in L-shell. These features are similar to the standing Alfvén wave events reported previously [e.g., *Sarris et al*., 2009; *Liu et al*., 2011; *Hartinger et al*., 2011]. The most interesting feature of this event is that the wave appears to exist only within the PBL region, marked by the two red vertical lines in Figure 2. This suggests that the existence of the ULF wave is likely associated with the observed PBL. The other two probes, TH-A and TH-E, observe similar feature, which confirms that the localization of the observed ULF wave is a spatial effect instead of a temporal effect.

[14] In Figure 2g, omnidirectional energy flux spectra of thermal ions from 1 to 30 keV are plotted, as measured by the ESA instrument. Before 15:45 UT, the instrument seems to be severely contaminated by penetrating high energy electrons, which can saturate the instrument or decrease the signal-to-noise ratio of the measurement as previously discussed by *McFadden et al*. [2008]. Outside the outer electron radiation belt, we can see that the energy flux of several to 10 keV ions is enhanced after 15:45 UT, suggesting possible bump-on-tail ion distributions, which will be discussed in detail with ion distribution function measurements in the next subsection.

[15] In order to analyze the harmonic mode of this wave, we investigate the phase difference between magnetic and electric field oscillations. In Figure 3, the 5–15 mHz band-pass-filtered signals of B_r and E_ϕ from TH-D are plotted for a shorter time range (15 min). By comparing the phase difference between the two components, we find that the phase of E_ϕ leads B_r by ~90°. Note that the satellite was north of the magnetic equator, so it is suggested that this event is an even harmonic standing wave [*Takahashi et al*., 2011].

3.2. Observation of Bump-on-Tail Distribution

[16] The bump-on-tail ion distribution functions, identified as positive *df/dW* gradients where *f* is the ion distribution function and *W* is particle energy, contain "free energy" that can be fed into a resonant wave mode through inverse Landau damping [e.g., *Southwood*, 1976]. The energy of the "bump," W_{bump}, is critical for determining resonance frequency. In this subsection, we use measurements of ion distribution functions by the ESA instrument of TH-D to obtain the information of W_{bump} during this event based on the method suggested by *Baddeley et al*. [2004]. Figures 4a and 4b show two examples of ion distribution functions calculated from omnidirectional flux measurements at 16:10 and 16:47 UT, respectively. In both figures, we can see the existence of positive *df/dW* gradient. The maximum and minimum energies of the positive gradient region are referred as W_{min} and W_{max}, as marked by the dashed line in both figures. W_{bump} is subsequently calculated by $W_{bump} = (W_{min} + W_{max})/2$.

[17] Figure 4c shows the results of W_{bump} investigation during this event from 15:00 to 17:00 UT. The observations of ion distribution function are plotted in the first panel. W_{bump} is calculated for the ion distribution functions with positive *df/dW* gradients between 1 and 15 keV, as shown in the second panel. The smoothed W_{bump} with a running time window of 10 min is plotted in the third panel. In the last panel, we show the comparison between the first and third panels to demonstrate the credibility of our method.

[18] As noted previously, ESA measurements before 15:45 UT are contaminated because of the encounter with the core of outer radiation belt, which leads to a low signal-to-noise ratio and prevents our analysis on W_{bump}. After 15:45 UT, W_{bump} value is shown to gradually decrease from

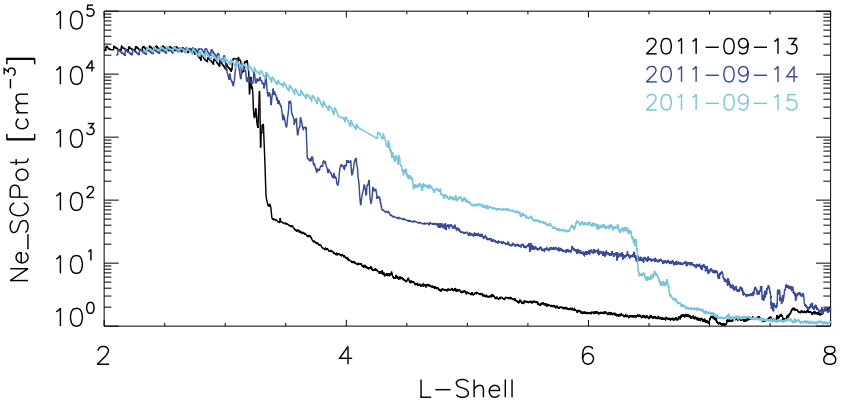

Figure 6. Electron density inferred from spacecraft potential versus L shell value during three successive outbound plasmapause crossings from 13 to 15 September 2011.

9.5 to 5.6 keV when the satellite travels from L = 5.2 to L = 6.5. The W_{bump} is plotted as a function of L value in Figure 5 for this event, which suggests a relation that can be described by a linear function

$$W_{bump}(in\ \mathrm{keV}) = 28 - 3.5 \times L \quad (1)$$

with a correlation coefficient of −0.98. The increase in W_{bump} with decreasing L value was also observed by *Wilson et al.* [2006] with polar measurements.

3.3. Evolution of the PBL

[19] In this subsection, we investigate the formation of the observed PBL by comparing the density profiles of three consecutive outbound passes from 13 to 15 September 2011, as shown in Figure 6. A moderate storm occurred on 9 September 2011 with a minimum *Dst* index of −74 nT. During the recovery phase on 13 September, TH-D crossed the plasmapause at L = 3.4, as indicated by a sharp density drop from 1.0×10^4 to 40 cm^{-3}, as shown by the black line in Figure 6. On 14 September, the plasmasphere started to expand and be refilled. On 15 September, the PBL described in section 3.1 was formed. The previous plasmapause expands to L = 4.4, corresponding to the inner boundary of the PBL. A new density gradient appeared at L = 6.5, corresponding to the outer boundary of the PBL. The electron density inside the PBL gradually decreases from ~200 to ~70 cm^{-3}.

4. Discussion

4.1. On the Harmonic Mode of the Poloidal Wave

[20] As discussed in the Introduction section, there are two techniques which have been widely used to identify the harmonic of a poloidal wave. In this subsection, we examine the harmonic mode of the observed poloidal oscillations based on these two methods.

[21] The first method compares the phase delay between radial magnetic field B_r and azimuthal electric field E_ϕ. In Figure 3, it is clearly shown that the phase of E_ϕ leads B_r by ~90° for measurements made slightly north of magnetic equator, suggesting an even harmonic mode.

[22] The second method compares the observed wave frequency with the theoretically calculated eigenfrequency of field lines for different polarization and harmonic. The data used in this analysis are plotted in Figure 7, with wavelet power spectra of B_r in Figure 7a and electron density in Figure 7b, respectively.

[23] The observed wave frequencies are extracted from the wavelet power spectra and plotted as the thick black line in Figure 7c. Here we search for the frequency at maximum power spectral density between 2 and 20 mHz for each time point with a requirement that the power spectra density is greater than 100 (nT)^2/Hz (corresponding to an amplitude of 1 nT for an oscillation of 10 mHz).

[24] The second harmonic poloidal frequencies are estimated based on the solutions of the decoupled transverse wave equations from previous studies by *Cummings et al.* [1969] and *Orr and Matthew* [1971]. *Cummings et al.* [1969] calculated the eigenfrequencies at geosynchronous orbit for different harmonics with asumptions including dipole magnetic field, cold plasma background, perfect ionospheric conductivity, and $n = n_{eq}(LR_E/R)^\gamma$ for the proton density distribution along field line, where n_{eq} is the proton density at magnetic equator of the field line, L is the L shell value, R_E is the radius of the Earth, R is the geocentric distance to a point on the field line, and γ is a power law index. *Orr and Matthew* [1971] expanded the solution for other L values. Based on their results, the eigenfrequency for the second harmonic poloidal mode at a given field line is proportional to $1/(n_{eq}^{1/2}L^4)$ if, for a simple estimation, one ignores the difference in the height where $E_r = E_\phi = 0$ above the Earth's surface. We adopt the second harmonic poloidal eigenfrequency of 38 mHz from *Cummings et al.* [1969] for $\gamma = 4$ at geosynchronous orbit calculated with $n_{eq} = 1$ cm^{-3}, and subsquently scale it to given L shells and observed electron density assuming all ions are protons. The result is plotted as the blue line in Figure 7c.

[25] From the comparison between the black and blue lines, it is evident that the observed wave frequency agrees well with the second harmonic frequency in the region where the waves are observed. We have tested other possible γ values and have found that, although $\gamma = 4$ reaches the best agreement with observations, other γ values also give resonable results; thus, the choice of γ value does not affect our conclusion. We should also note here that although the

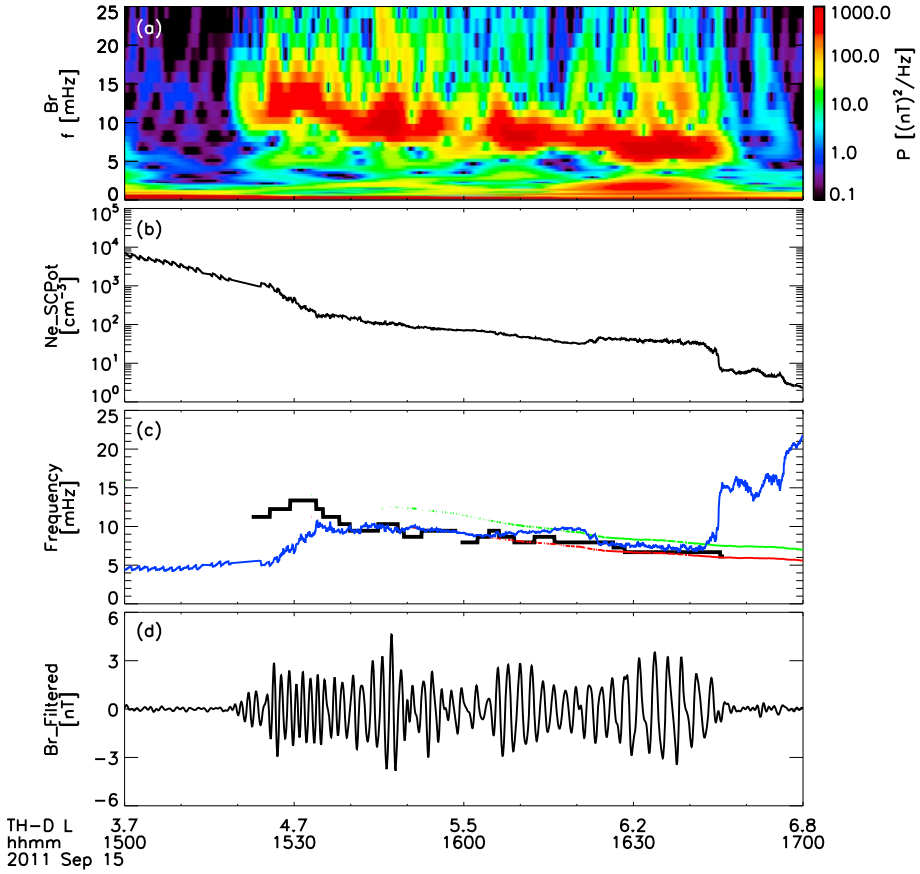

Figure 7. (a) Wavelet power spectra of the radial component of magnetic field in the MFA coordinate system observed by TH-D; (b) Electron density derived from the spacecraft potential measurement from TH-D; (c) Comparison of frequencies: observed wave frequency in black, second harmonic poloidal eigenfrequency in blue, and bounce frequencies of protons with observed W_{bump} for 30 and 60° pitch angle in red and green, respectively; (d) Band-pass-filtered signal of radial magnetic field observed by TH-D.

agreement in this paper seems to be resonable, the estimation here is still rough. The biggest uncertainty in our calculation might be due to the assumption that all ions are protons, since the heavy ion populations can increase the ion mass density, decrease the Alfvén velocity, and thus affect the eigenfrequencies. A more accurate calculation should involve modeling considering wave damping by the ionosphere [*Newton et al*., 1978], a realistic magnetic field model [*Singer et al*., 1981], and using mass density instead of electron density [*Takahashi et al*., 2004; *Denton et al*., 2006].

[26] Overall, the first method suggests that the observed ULF waves are in even harmonic mode. The second method excludes the possibility of the harmonic modes higher than second harmonic. For example, the fourth harmonic mode has an eigenfrequency roughly twice of the eigenfrequency of second harmonic, which does not agree with observations. Thus, based on the above analysis, we confidently conclude that the observed ULF waves in the PBL are second harmonic poloidal oscillations.

4.2. On the Generation Mechanism of the Poloidal Wave

[27] The generation mechanism of poloidal ULF waves has been extensively studied. Several mechanisms have been proposed, either from external or internal sources. Poloidal waves generated by an external source usually last for a short time period (several cycles), have low m number, and strong compressional component [e.g., *Zong et al*., 2009a, *Du et al*., 2010], which are quite different from the observation presented in this paper. For internal sources, there are two generation mechanisms that have also been considered. One is the drift resonance [*Southwood*, 1976], with inward gradient of ion phase space density. Waves generated by this mechanism are expected to be odd modes, which is not what is observed during this event. The other mechanism is the drift-bounce resonance with bump-on-tail hot ion distribution [*Southwood*, 1976; *Hughes et al*., 1978]. Waves generated by this mechanism are in even mode, which is consistent with the observations in this event. This feature, along with the presence of a bump-on-tail ion distribution, suggests that drift-bounce resonance is likely the generation mechanism of the observed second harmonic poloidal wave.

[28] The condition of drift-bounce resonance is described in *Southwood* [1976] as,

$$\omega - m\omega_D = N\omega_B \tag{2}$$

where ω is the wave frequency, ω_D is the particle drift frequency, ω_B is the particle bounce frequency, m is the azimuthal wave

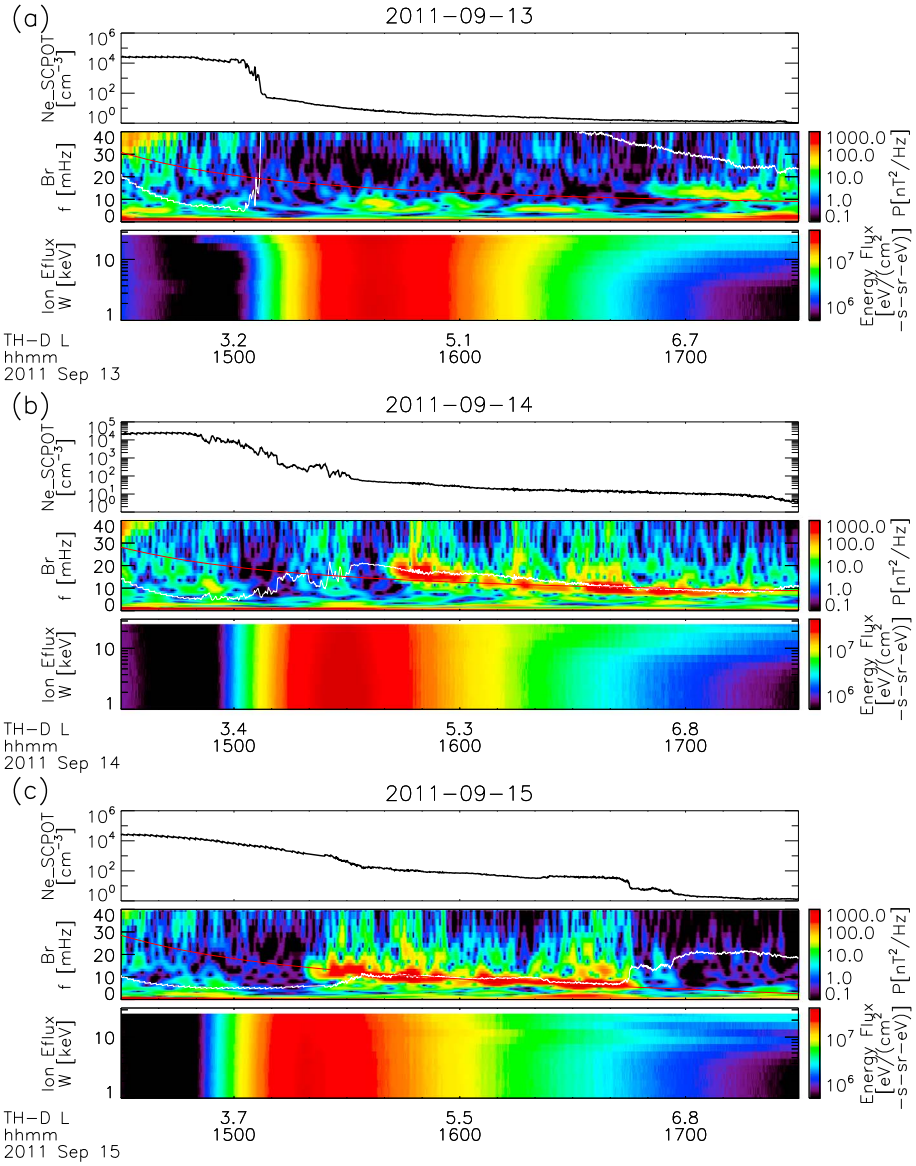

Figure 8. (a) Time series of inferred electron density in the top panel, wavelet power spectra of radial magnetic field in the middle panel and ion energy spectra in the bottom panel observed by TH-D for 13 September 2011. Eigenfrequency of second harmonic poloidal mode (white line) and bounce frequency of the particle with bump energy and 30° pitch angle (red line) are plotted on top of the wave power spectra; (b) Same as Figure 8a but for 14 September 2011; (c) Same as Figure 8a but for 15 September 2011.

number, and N is an integer (usually ±1). In a dipole field, ω_D and ω_B can be estimated as [e.g., *Roederer*, 1970]

$$\omega_D \approx L \cdot W \cdot R_E(0.7 + 0.3\sin\alpha)/120qk_0$$
$$\omega_B \approx \frac{\sqrt{2W/m_i}}{4LR_E(1.3 - 0.56\sin\alpha)} \quad (3)$$

where W is particle energy, q is electric charge of a particle, k_0 is the magnetic moment of Earth's dipole, α is the particle's equatorial pitch angle, and m_i is the ion mass. The approximate solutions of equation (2) for $|N| = 1$ are $\omega \sim \omega_B$ (low-energy resonance) and $m\omega_D \sim \omega_B$ (high-energy resonance) [e.g., *Southwood*, 1976]. In the following, we assume that the low-energy resonance is relevant to our poloidal wave event. This is the same type of resonance as the "drift-bounce resonance" that *Hughes et al.* [1978] reported first.

[29] In Figure 7c, we plot the bounce frequencies calculated for the protons with energy of observed W_{bump}, i.e., the energy at the positive slope of the observed bump-on-tail ion distribution. The red and green lines represent the result for particles with 30 and 60° pitch angle, respectively. The bounce frequencies are close to the observed wave frequency, and their trends are similar, which confirms that the observed waves are generated by drift-bounce resonance with $|N| = 1$.

4.3. On the Source of the Hot Ions

[30] In this event, ions in a narrow energy range of ~10 keV are observed penetrating deeply into the region of L ~ 3. This type of structure has been referred as nose-like structure and has been extensively studied since it was first observed by

Smith and Hoffman [1974]. A statistical study [*Vallat et al*., 2007] found that nose-like structures appear regardless of geomagnetic activity level and MLT sector. The formation of nose-like structures is suggested to be a result of the drift of particles from the plasma sheet under global-scale electric fields [*Zong et al*., 2009b; *Wang and Zong*, 2012].

[31] Hot ions of nose-like structures can create bump-on-tail ion distributions. Their energies (~10 keV) are preferential for the resonance condition required by drift-bounce resonance [*Hughes et al*., 1978]. Based on polar observations, *Baddeley et al*. [2004] statistically studied the free energy associated with non-Maxwellian proton distributions in the inner magnetosphere and found that ~10 to 40 keV protons contain the highest free energy. *Baddeley et al*. [2005b] further statistically demonstrated that the particle populations observed during conjugate ionospheric high *m* wave events have more free energy available than populations extracted at random. In our paper, we show that strong poloidal ULF waves are generated with the presence of nose-like structure, suggesting that nose-like structures can impact ULF wave generation by providing energy for the drift-bounce resonance.

4.4. On the Effect of the PBL

[32] During magnetic storms, enhanced convection compresses plasmasphere and moves the plasmapause to lower radial distances [e.g., *Baker et al*., 2004]. After storms, the plasmasphere starts to expand and to be refilled [e.g., *Fu et al*., 2010]. The inferred plasma density, the wavelet power spectra of B_r, and ion energy spectra for the three consecutive outbound orbits from 13 to 15 September 2011 are plotted in Figures 8a–8c. There are two interesting features in this figure.

[33] First, it is shown from the wave power spectra that monochromatic ULF pulsations are observed only at certain locations, as shown in Figure 8. As shown from the ion energy spectra, bump-on-tail distributions are observed for all the three orbits, providing necessary conditions for drift-bounce resonance. The drift-bounce resonance should be coupled with local standing Alfvén wave; otherwise, the excited waves would be damped quickly. Standing ULF waves can be observed at the locations where the drift-bounce resonance frequency matches the local eigenfrequency and/or its harmonics. On top of each wave power spectra in Figure 8, two lines are plotted. The white line represents the eigenfrequency of second harmonic poloidal mode, and the red line represents the bounce frequency of particles with bump energy and 30° pitch angle. Note that the bump energy is different for the three days. We use an estimation of 15.7 keV for 13 and 14 September and use equation (1) for 15 September in the calculation. As clearly shown in Figure 7c and Figure 8, the second harmonic poloidal oscillations are excited in the region where the eigenfrequency is close to bounce frequency, but not in the region where the eigenfrequency deviates from bounce frequency. Our hypothesis also explains the observations by *Singer et al*. [1982], who noticed disappearance of poloidal waves at the region of low plasma density but was not able to conclude whether it was a temporal or spatial effect.

[34] Second, different from the observation on 15 September, the boundaries of wave activity on 13 and 14 September are not associated with density gradients. This suggests that the presence of a sharp density gradient is not a necessary condition for the excitation of the observed poloidal waves.

[35] We further argue that cold plasma density seems to be a controlling factor for ULF wave generation that can regulate the location where the ULF wave can be excited by changing the local field line eigenfrequency to match resonance conditions. The cold plasma density has been considered to vary regularly with geocentric distance or L shell value [e.g., *Orr and Matthew*, 1971]. In the plasma trough region, the plasma density can be assumed to vary inversely as the fourth power of L, while a smaller power law index is usually assumed inside the plasmasphere. However, in the PBL region, where the cold plasma density can have complicated variations, its effect on regulating ULF wave excitation becomes more important.

5. Conclusions

[36] A poloidal ULF wave event generated in the PBL has been investigated in this paper. After a moderate storm, the plasmasphere expands and a PBL with two density gradients is formed. Intense poloidal ULF waves are observed inside the PBL region. We have demonstrated that the observed ULF waves are second harmonic poloidal oscillations generated by drift-bounce resonance with bump-on-tail plasma distribution at ~10 keV. We have found that the waves are excited only at the locations where the eigenfrequency of second harmonic is close to the bounce frequency, suggesting that cold plasma density seems to control the locations where the ULF waves can be excited by matching the local eigenfrequency of field lines with resonance conditions. The complicated plasma density variations in the PBL can enhance ULF wave generation by changing the eigenfrequency of field lines.

[37] **Acknowledgments.** This work was supported by NSFC grants (41104109 and 41274166), NASA grant (NNX10AQ48G), and the Specialized Research Fund for State Key Laboratories (201203FSK05). Work at Beihang University was in part supported by 973 program of China (2011CB811404). Work at JHU/APL was supported by NASA grant NNX10AK93G. We thank U. Auster for the use of THEMIS/FGM data, J. W. Bonnell for the use of THEMIS/EFI data, and J. McFadden for the use of THEMIS/ESA data. THEMIS mission is supported by NASA (NAS5-02099).

[38] Robert Lysak thanks Tim Yeoman and another reviewer for their assistance in evaluating this paper.

References

Anderson, B. J., M. J. Engebretson, S. P. Rounds, L. J. Zanetti, and T. A. Potemra (1990), A statistical study of Pc3-5 pulsations observed by the AMPTE/CCE magnetic field experiment 1, Occurrence distributions, *J. Geophys. Res.*, *95*(A7), 10,495–10,523.

Angelopoulos, V. (2008), The THEMIS Mission, *Space Sci. Rev.*, doi:10.1007/s11214-008-9336-1.

Arthur, C. W., and R. L. McPherron (1981), The statistical character of Pc4 magnetic pulsations at synchronous orbit, *J. Geophys. Res.*, *86*(A3), 1325–1334.

Auster, H. U., et al. (2009), The THEMIS Fluxgate Magnetometer, *Space science reviews*, *141*(1-4), 235–264.

Baddeley, L. J., T. K. Yeoman, D. M. Wright, K. J. Trattner, and B. J. Kellet (2004), A statistical study of unstable particle populations in the global ring current and their relation to the generation of high m ULF waves, *Ann. Geophys.*, *22*, 4229–4241.

Baddeley, L. J., T. K. Yeoman, and D. M. Wright (2005a), HF Doppler sounder measurements of the ionospheric signatures of small scale ULF waves, *Ann. Geophys.*, *23*(5), 1807–1820, doi:10.5194/angeo-23-1807-1820.

Baddeley, L. J., T. K. Yeoman, D. M. Wright, K. J. Trattner, and B. J. Kellet (2005b), On the coupling between unstable magnetospheric particle populations and resonant high m ULF wave signatures in the ionosphere, *Ann. Geophys.*, *23*, 567–577, doi:10.5194/angeo-23-567-2005.

Baker, D. N., S. G. Kanekal, X. Li, S. P. Monk, J. Goldstein, and J. L. Burch (2004), An extreme distortion of the Van Allen belt arising from the/ Hallowe'en/'solar storm in 2003. *Nature 432*(7019), 878–881.

Bonnell, J. W., F. S. Mozer, G. T. Delory, A. J. Hull, R. E. Ergun, C. M. Cully, V. Angelopoulos, and P. R. Harvey (2008), "The electric field instrument (EFI) for THEMIS," *Space Science Reviews 141*(1-4), 303–341.

Cao, J.-B., et al. (2008), Characteristics of middle-to-low latitude Pi2 excited by bursty bulk flows, *J. Geophys. Res.*, *113*, A07S15, doi:10.1029/ 2007JA012629.

Cao, J.-B., et al. (2010), Geomagnetic signatures of current wedge produced by fast flows in a plasma sheet, *J. Geophys. Res.*, *115*, A08205, doi:10.1029/2009JA014891.

Carpenter, D. L., and J. Lemaire (2004), The plasmasphere boundary layer, *Ann. Geophys.*, *22*, 4291.

Chen, L., and A. Hasegawa (1991), Kinetic theory of geomagnetic pulsations, 1, Internal excitation by energetic particles, *J. Geophys. Res.*, *96*(A2), 1503–1512.

Cummings, W. D., R. J. O'Sullivan, and P. J. Jr.Coleman (1969), Standing Alfvén waves in the magnetosphere, *J. Geophys. Res.*, *74*(3), 778–793.

Denton, R. E., K. Takahashi, I. A. Galkin, P. A. Nsumei, X. Huang, B. W. Reinisch, R. R. Anderson, M. K. Sleeper, and W. J. Hughes (2006), Distribution of density along magnetospheric field lines, *J. Geophys. Res.*, *111*, A04213, doi:10.1029/2005JA011414.

Du A. M., et al. (2010), Experimental evidence of direct penetration of upstream ULF waves from the solar wind into the magnetosphere during the strong magnetic storm of November 9, 2004, *Planet. Space Sci.*, *58*(7-8), June 2010, 1040–1044.

Fu, H. S., J. Tu, P. Song, J. B. Cao, B. W. Reinisch, and B. Yang (2010), The nightside-to-dayside evolution of the inner magnetosphere: Imager for Magnetopause-to-Aurora Global Exploration Radio Plasma Imager observations, *J. Geophys. Res.*, *115*, A04213, doi:10.1029/2009JA014668.

Hartinger, M., et al. (2011), Global energy transfer during a magnetospheric field line resonance, *Geophys. Res. Lett.*, *38*, L12101, doi:10.1029/ 2011GL047846.

Hughes, W. J., et al. (1978), Alfvén waves generated by an inverted plasma energy distribution, *Nature*, *275*, 43–45, doi:10.1038/275043a0.

Kozlov, D. A., et al. (2006), The structure of standing Alfven waves in a dipole magnetosphere with moving plasma, *Annales Geophysicae*, *24*(1), 263–274.

Leonovich, A. S., et al. (2008), Standing Alfvén waves with m>> 1 in a dipole magnetosphere with moving plasma and aurorae, *Adv. Space Res.*, *42*(5), 970–978.

Li, X., et al. (2006), Correlation between the inner edge of outer radiation belt electrons and the innermost plasmapause location, *Geophys. Res. Lett.*, *33*, L14107, doi:10.1029/2006GL026294.

Li, W., et al. (2010), Global distributions of superthermal electrons observed on THEMIS and potential mechanisms for access into the plasmasphere, *J. Geophys. Res.*, *115*, A00J10, doi:10.1029/2010JA015687.

Liu, W., et al. (2009), Electric and magnetic field observations of Pc4 and Pc5 pulsations in the inner magnetosphere: A statistical study, *J. Geophys. Res.*, *114*, A12206, doi:10.1029/2009JA014243.

Liu, W., et al. (2011), Spatial structure and temporal evolution of a dayside poloidal ULF wave event, *Geophys. Res. Lett.*, *38*, L19104, doi:10.1029/ 2011GL049476.

McFadden, J. P., et al. (2008), The THEMIS ESA plasma instrument and in-flight calibration, *Space Sci. Rev.*, *141*, 277–302, doi:10.1007/s11214-008-9440-2.

McIlwain, C. E. (1961), Coordinates for mapping the distributions of magnetically trapped particles, *J. Geophys. Res.*, *66*, 3681–3691.

Moldwin, M. B., and S. Zou (2012), The Importance of the Plasmasphere Boundary Layer for Understanding Inner Magnetosphere Dynamics, *Geophysical Monograph Series*, *199*, 321–327.

Moldwin, M. B., et al. (2002) A new model of the location of the plasmapause: CRRES results, *J. Geophys. Res.*, *107*(A11), 1339, doi:10.1029/2001JA009211.

Newton, R. S., D. J. Southwood, and W. J. Hughes (1978), Damping of geomagnetic pulsations by the ionosphere, *Planet. Space Sci.*, *26*, 201–209.

Orr, D., and J. A. D. Matthew (1971), The variation of geomagnetic micro-pulsation periods with latitude and the plasmapause, *Planet. Space Sci.*, *19*, 897–905, doi:10.1016/0032-0633(71)90141-3.

Pedersen, A., et al. (1998), Electric field measurements in a tenuous plasma with spherical double probes, in *Measurement Techniques in Space Plasmas: Fields*, Geophys. Monogr. Ser., vol. *103*, edited by R. F. Pfaff, J. E. Borovsky, and D. T. Young, pp. 1–12, AGU, Washington, D. C.

Roederer, J. G. (1970). Dynamics of geomagnetically trapped radiation, in *Physics and Chemistry in Space*, 52–58, Springer, Berlin.

Sarris T. E., et al. (2009), Characterization of ULF pulsations by THEMIS, *Geophys. Res. Lett.*, *36*, L04104, doi:10.1029/2008GL036732.

Sarris, T. E., et al. (2010), THEMIS observations of the spatial extent and pressure-pulse excitation of field line resonances, *Geophys. Res. Lett.*, *37*, L15104, doi:10.1029/2010GL044125.

Shue, J.-H., et al. (1998), Magnetopause location under extreme solar wind conditions, *J. Geophys. Res.*, *103*(A8), 17,691–17,700, doi:10.1029/98JA01103.

Singer, H. J., D. J. Southwood, R. J. Walker, and M. G. Kivelson (1981), Alfvén wave resonances in a realistic magnetospheric magnetic field geometry, *J. Geophys. Res.*, *86*, 4589–4596.

Singer, H. J., J. W. Hughes, and C. T. Russell (1982), Standing hydromagnetic waves observed by ISEE 1 and 2: radial extent and harmonic, *J. Geophys. Res.*, *87*(A5), 3519–3529.

Smith, P. H., and R. A. Hoffman (1974), Direct Observations in the Dusk Hours of the Characteristics of the Storm Time Ring Current Particles During the Beginning of Magnetic Storms, *J. Geophys. Res.*, *79*(7), 966–971, doi:10.1029/JA079i007p00966.

Southwood, D. J. (1976), A general approach to low-frequency instability in the ring current plasma, *J. Geophys. Res.*, *81*, 3340–3348, doi:10.1029/ JA081i019p03340.

Takahashi, K., and B. J. Anderson (1992), Distribution of ULF energy (f 80 mHz) in the inner magnetosphere: A statistical analysis of AMPTE CCE magnetic field data, *J. Geophys. Res.*, *97*(A7), 10,751–10,773.

Takahashi, K., R. W. McEntire, A. T. Y. Lui, and T. A. Potemra (1990), Ion flux oscillations associated with a radially polarized transverse Pc5 magnetic pulsation, *J. Geophys. Res.*, *95*(A4), 3717–3731.

Takahashi, K., R. E. Denton, R. R. Anderson, and W. J. Hughes (2004), Frequencies of standing Alfvn wave harmonics and their implication for plasma mass distribution along geomagnetic field lines: Statistical analysis of CRRES data, *J. Geophys. Res.*, *109*, A08202, doi:10.1029/2003JA010345.

Takahashi, K., et al. (2011), Multisatellite observations of a giant pulsation event, *J. Geophys. Res.*, *116*, A11223, doi:10.1029/2011JA016955.

Vallat, C., et al. (2007), Ion multi-nose structures observed by Cluster in the inner magnetosphere, *Ann. Geophys.*, *25*, 171–190.

Wang, Y. F., and Q.-G. Zong (2012), Study of the nose event on 11 April 2002 with UBK method, *Sci. China Technol. Sci.*, *55*, 1929–1942, doi:10.1007/s11431-012-4862-1.

Wilson, M. E., T. K. Yeoman, L. J. Baddeley, and B. J. Kellet (2006), A statistical investigation of the invariant latitude dependence of unstable magnetospheric ion populations in relation to high m ULF wave generation, *Ann. Geophys.*, *24*, 3027–3040, doi:10.5194/angeo-24-3027-2006.

Zong, Q.-G., et al. (2009a), Energetic electron response to ULF waves induced by interplanetary shocks in the outer radiation belt, *J. Geophys. Res.*, *114*, A10204, doi:10.1029/2009JA014393

Zong, Q.-G., et al. (2009b), Vortex-like plasma flow structures observed by Cluster at the boundary of the outer radiation belt and ring current: A link between the inner and outer magnetosphere, *J. Geophys. Res.*, *114*, A10211, doi:10.1029/2009JA014388.